Fall 2016

Identifying the shape collapse problem in large deformation image registration

Wei Shao
University of Iowa

IDENTIFYING THE SHAPE COLLAPSE PROBLEM IN LARGE DEFORMATION IMAGE REGISTRATION

by

Wei Shao

A thesis submitted in partial fulfillment of the
requirements for the Master of Science
degree in Electrical and Computer Engineering
in the Graduate College of
The University of Iowa

December 2016

Thesis Supervisor: Professor Gary E. Christensen

Graduate College
The University of Iowa
Iowa City, Iowa

CERTIFICATE OF APPROVAL

MASTER'S THESIS

This is to certify that the Master's thesis of

Wei Shao

has been approved by the Examining Committee for the thesis requirement for the Master of Science degree in Electrical and Computer Engineering at the December 2016 graduation.

Thesis committee: _____
Gary E. Christensen, Thesis Supervisor

_____
Hans J. Johnson

_____
Oguz C. Durumeric

ACKNOWLEDGEMENTS

I would first like to express my sincere gratitude to my thesis advisor Professor Gary Christensen of the Electrical and Computer Engineering Department at the University of Iowa for his valuable guidance through the learning process of this master thesis. Whenever I had questions about my research or courses, Professor Christensen was ready to provide me with insightful advice and teach me to solve the problem.

Second, I would like to thank Professor Hans Johnson for his great class about using ITK for higher dimensional image processing, and kindly teaching me to use the tool BRAINS AutoWorkup to perform image registration.

Third, I would like to thank Professor Oguz Durumeric for patiently providing me with insightful mathematical guidance for my thesis.

Fourth, I would like to thank Doctors Vincent Magnotta and Joseph Shaffer for pointing out the artifacts in the image registration used for the bipolar disorder project. Then Professor Gary Christensen suggested that these artifacts may caused by shape collapse, which inspired me to study the main topic of my thesis, the shape collapse problem in large deformation image registration.

I would also like to thank my colleagues and friends Yue Pan, Bowen Zhao, Joo Hyun Song, Ali Gayhoor, Regina Kim, Professor Casey Johnson, Doctor Jess Fiedorowicz and Professor John Wemmie for their kind help and friendship.

Finally, I want to thank my father Rongan Shao, my mother Aixiu Sun and

my brother Xiao Shao for their support and understanding for the past two years.

This work was supported by the generous donation provided by Roger Koch.

ABSTRACT

This thesis examines and identifies the problems of shape collapse in large deformation image registration. Shape collapse occurs in image registration when a region in the moving image is transformed into a set of near zero volume in the target image space. Shape collapse may occur when the moving image has a structure that is either missing or does not sufficiently overlap the corresponding structure in the target image [6]. We state that shape collapse is a problem in image registration because it may lead to the following consequences: (1) Incorrect pointwise correspondence between different coordinate systems; (2) Incorrect automatic image segmentation; (3) Loss of functional signal. The above three disadvantages of registration with shape collapse are illustrated in detail using several examples with both real and phantom data. Shape collapse problem is common in image registration algorithms with large degrees of freedom such as many diffeomorphic image registration algorithms. This thesis proposes a shape collapse measurement algorithm to detect the regions of shape collapse after image registration in pairwise and group-wise registrations. We further compute the shape collapse for a whole population of pairwise transformations such as occurs when registering many images to a common atlas coordinate system. Experiments are presented using the SyN diffeomorphic image registration algorithm and diffeomorphic demons algorithm. We show that shape collapse exists in both of the two large deformation registration methods. We demonstrate how changing the input parameters to the SyN registration algorithm can mitigate the collapse image

registration artifacts.

PUBLIC ABSTRACT

Image registration is the process of finding a geometric transformation that defines an optimal pointwise correspondence between a moving image and a target image (fixed image). This correspondence transformation deforms the moving image into the shape of the target image.

This thesis mainly examines the problems of shape collapse in image registration with large degrees of freedom for its transformation function. Shape collapse occurs in image registration when some structure with nonzero volume in the moving image is transformed into a set of near zero volume in the target image space. Shape collapse may occur when the moving image has a structure that is either missing or does not sufficiently overlap the corresponding structure in the target image [6]. We state that shape collapse is a problem in image registration because it may lead to the following consequences: (1) Incorrect pointwise correspondence between moving image and target image, for example, a point in the white matter in the moving image was mapped to a point in the gray matter in the target image; (2) Incorrect automatic image segmentation, which is to deform the label map of the moving image into the target image space using the generated transformation to obtain a segmentation of the target image; (3) Loss of functional signal, which may occur when mapping functional data such as fMRI, PET, SPECT using a transformation with a shape collapse if the functional signal occurs at the collapse region. The above three disadvantages of registration with shape collapse are illustrated in detail using several

examples. We demonstrate that shape collapse is common in large deformation image registration. This thesis proposes a shape collapse measurement algorithm to detect regions in the target image space that have shape collapse problem after pairwise image registration. Each pairwise registration may exhibit the collapse problem. We evaluate the percentage of whole population that has a shape collapse at each point in the target image space. By evaluating the shape collapse for a population of pairwise transformations and generating a population shape collapse probability map. We show that shape collapse exists in both the SyN diffeomorphic and the diffeomorphic demons large deformation image registration methods. We demonstrate that changing the input parameters to the SyN registration algorithm can mitigate the collapse image registration artifacts. Finaly, we show that reducing the shape collapse may not necessarily solve the poor correspondence problem.

TABLE OF CONTENTS

LIST OF TABLES

Table

LIST OF FIGURES

Figure

CHAPTER 1
INTRODUCTION

The goal of medical image registration is to find a one-to-one mapping between two different coordinate systems such that points correspond to the same biological structure are mapped to each other [15]. Applications of medical image registration include automatic image segmentation [16][7][5]; radiation theory [17][19][12]; combining different imaging modalities of the same subject [4][14][11].

Durumeric, Oguz and Christensen [6] were the first to investigate the shape collapse problem in image registration. Shape collapse occurs when a foreground or background structure in the moving image with non-zero volume is transformed into a set of near zero volume in the target image coordinate system [6]. This may be a desirable property if the structure does not exist in the target image, i.e., no correspondence exists if a structure is present in the moving image but does not exist in the target image. However, a collapse is not desirable if a structure or part of a structure with non-zero volume present in the moving image is mapped to a set of near zero volume rather than to its corresponding location in the target image. In the later case, the estimated transformation defines an inaccurate pointwise correspondence between the moving and target image. Inaccurate correspondence is a problem when one wants to map information from the coordinate system of the moving image to the coordinate system of the target image. For example, it is common to use the correspondence transformation to map object names/labels or functional data such as fMRI, PET, and SPECT from one image coordinate system to another.

One type of shape collapse problem is illustrated in Fig. 1.1 by image registration of two MR images of the brain. Two 3D T1-weighed MR images of the brain were registered using the symmetric diffeomorphic image (SyN) registration [1] method developed by B.B. Avants *et al.* and is distributed as part of the Automatic Normalization Toolkit (ANTs) [2]. In this example, the T1 image shown in Fig. 1.1a was registered to the image shown in Fig. 1.1b; Figs. 1.1c and 1.1d show the resulting deformed moving images. The red circles show regions of shape collapse. Notice that the cerebral cortex inside the red circles in the deformed image appear to have collapsed in order to match the target image in these regions, which does not contain such cortical structure in those regions. Small regions of shape collapse like these are often hard to detect and are often over looked. However, if this transformation is used to map information from the moving image coordinate system to that of the target image, any information such as structure labels or functional brain response would map to a much smaller region in the target coordinate system. It is even possible that all information could be lost if an entire region of interest in the moving image of non-zero volume is mapped to a region of zero volume in the target image coordinate system. Another problem with transformations that contain regions of shape collapse is that they produce incorrect correspondences in the vicinity of the shape collapse.

We note that shape collapse image registration artifacts like those shown in Fig. 1.1 are produced by many diffeomorphic image registration algorithms. We chose to mainly study the SyN registration algorithm in this paper since it is publicly available and because it is used in the BRAINS AutoWorkup pipeline (Brain Research:

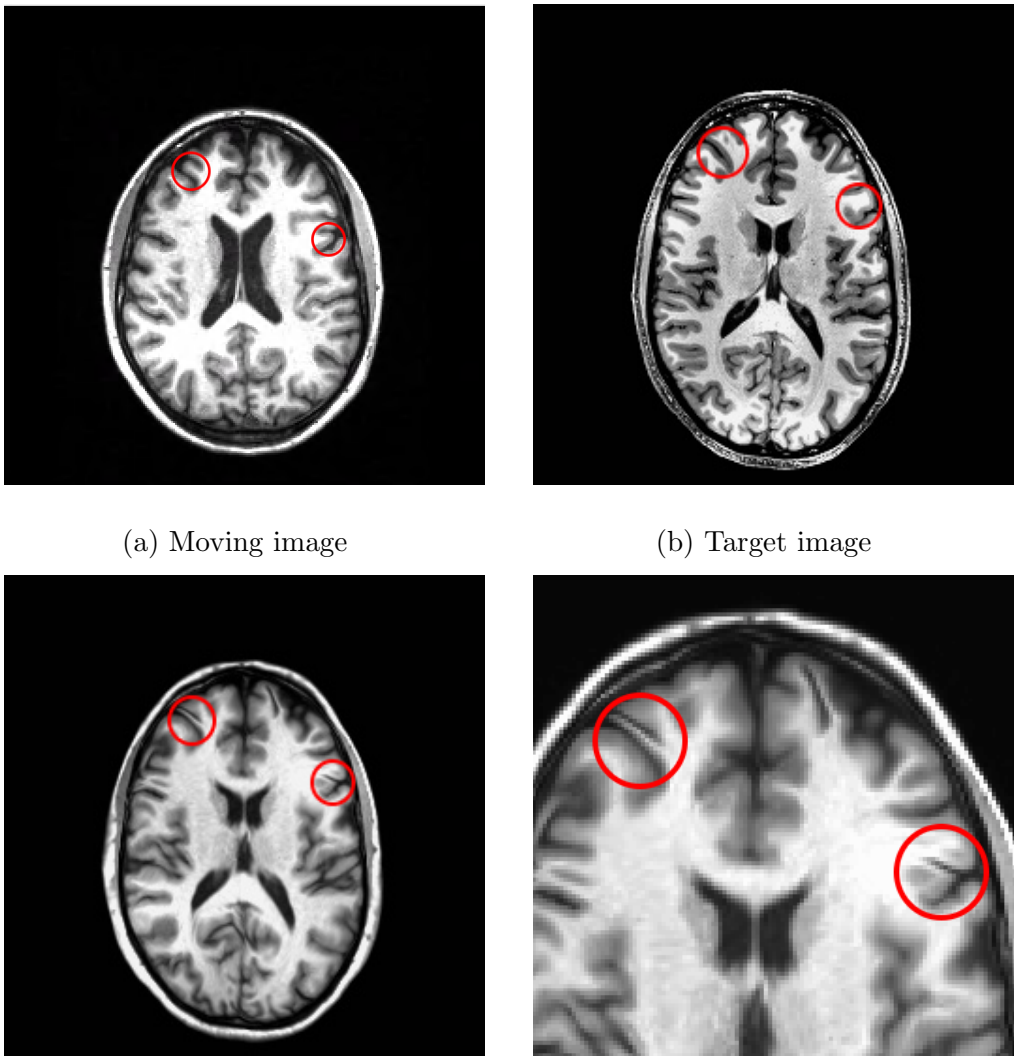

(a) Moving image

(b) Target image

(c) Deformed moving image

(d) Collapsed regions

Figure 1.1: Demonstration of shape collapse problem in pairwise 3D MR brain image registration. Panel: a. Transverse slice of moving image, b. Transverse slice of the target image, c. Deformed moving image, collapse regions shown inside red circles, d. Closer view of panel c.

Analysis of Images, Networks, and systems [13]) that is commonly used to nonrigidly register brain images. We will also study the shape collapse problem using another large deformation image registrant method, diffeomorphic demons algorithm [21], which is available in Insight Toolkit (ITK). We use a simple 2D brain cortex phantom example shown in Fig.1.2 to illustrate another type of shape collapse that may occur using common diffeomorphic image registration algorithms. The white object in these phantoms corresponds to a simplified cortex shape with a single sulcus in the transverse orientation. The cortex in the moving image does not fully overlap with the cortex in the target image. When using symmetric diffeomorphic registration (SyN) with normalized cross correlation similarity cost function, the non-overlapped cortex in the moving image collapsed to a set of near zero volume and a new cortex grew out to match the non-overlapped cortex in the target image (see Fig.1.2e). The desired transformation to match the moving image with the target image is a local rigid rotation of the cortex in the moving image. A small collapse artifact that is often ignored can be seen in Fig.1.2f at the bottom part of the deformed sulcus. Red and arrows in the intermediate deformed moving image shows the directions of cortex in the moving image collapsed new cortex grew out, respectively. To give more details of how the cortex collapsed during registration, we select some intermediate deformed images, which are shown in Fig.1.3.

The reason the shape collapse problem exists in the above case is that the greedy similarity cost reduces immediately when the non-overlapped cortex collapses or grows out instead of rotating. Therefore, shape collapse is a common problem for

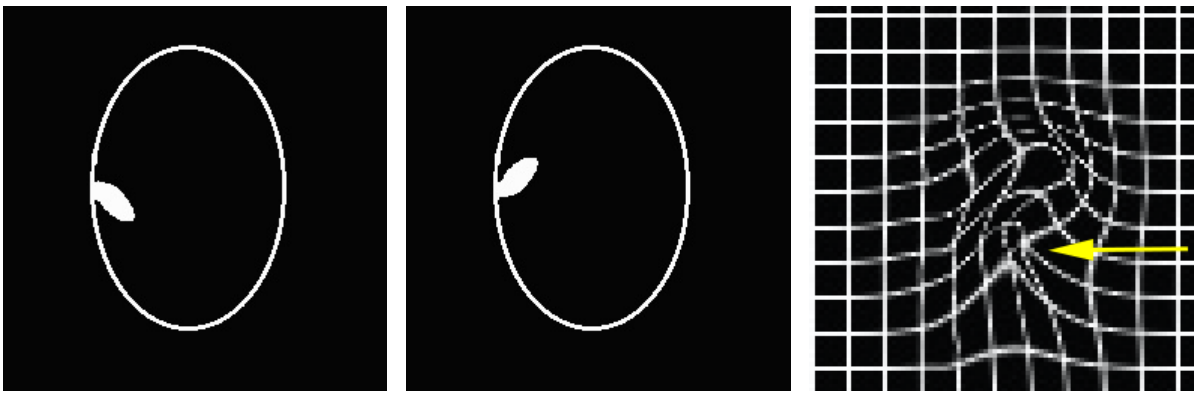

(a) Moving phantom image

(b) Target phantom image

(c) Final deformed grid; zoomed on ROI

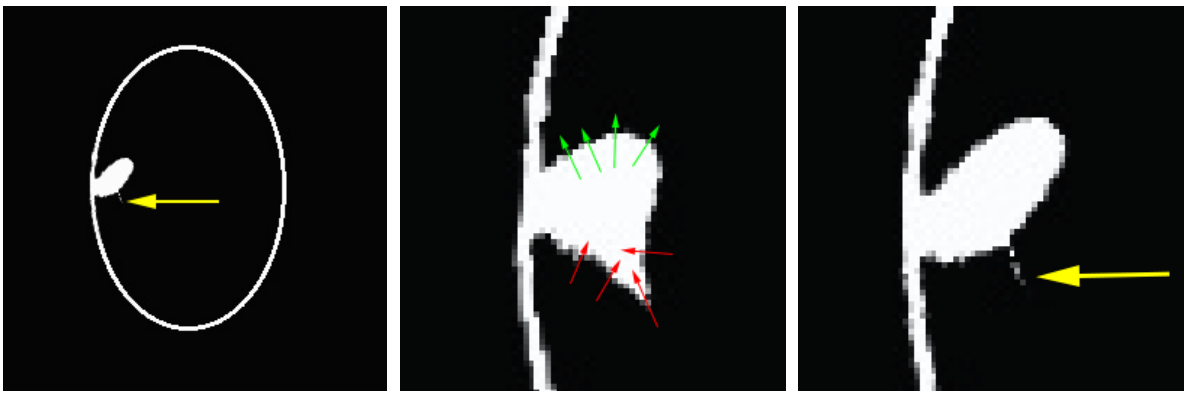

(d) Deformed moving image

(e) Intermediate deformed moving image; zoomed on ROI

(f) Final deformed moving image; zoomed on ROI

Figure 1.2: A simple 2D cortex phantom example to explain shape collapse when using diffeomorphic image registration. The cortex in this example has a single sulcus which we will call the region of interest (ROI). Notice that panels b and d look similar and do not appear to have a collapse. Zooming in on the ROI in panels e and f show that sulcus in the moving image did not rotate to match the target sulcus, but rather it collapsed at the bottom and grew from the top.

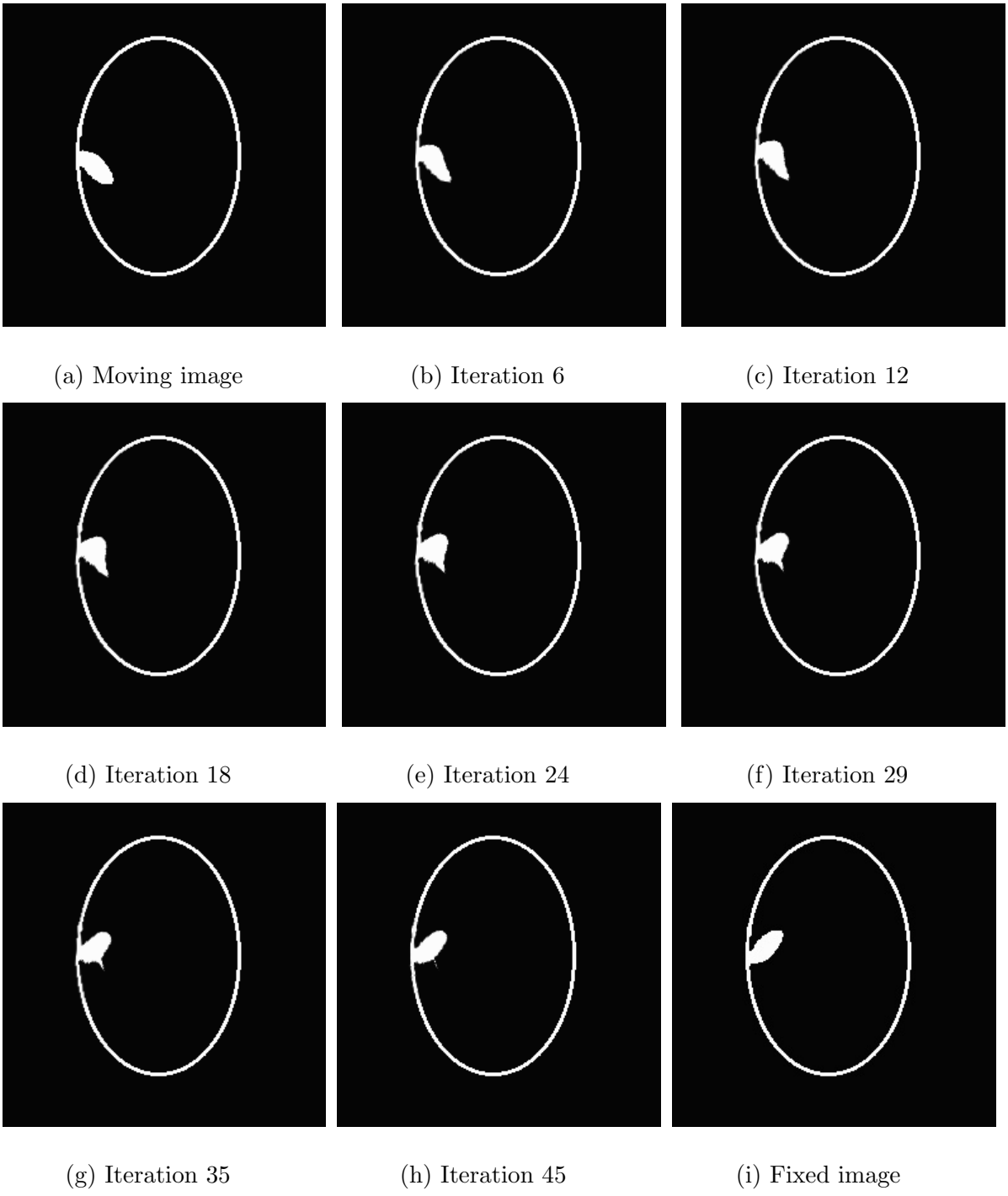

(a) Moving image (b) Iteration 6 (c) Iteration 12

(d) Iteration 18 (e) Iteration 24 (f) Iteration 29

(g) Iteration 35 (h) Iteration 45 (i) Fixed image

Figure 1.3: Flow of deformation of the phantom cortex using SyN registration.

image registration methods using greedy cost functions.

The reason shape collapse problem is often overlooked or ignored is that when investigating the quality of a registration algorithm, the primarily interest is whether the deformed moving image and the target image look similar to each other or not, without carefully looking at the point-to-point correspondences defined by the correspondence transformation.

The BRAINS AutoWorkup (BAW) [13], is a NiPype (Neuroimaging in Python Pipelines and Interfaces) based workflow that provides an automated procedure for large-scale multi-center longitudinal MR image analysis; this includes denoising, spatial normalization, intra-subject alignment, tissue classification, bias-field correction, and structure segmentation.

In this paper, we mainly investigate the shape collapse problem in MR brain image registration using BRAINS AutoWorkup pipeline, for which symmetric diffeomorphic image registration is part of its image registration process. We will also examine shape collapse problem using the diffeomorphic demons algorithm [21]. We will identify the problems of shape collapse in large deformation registration in detail. We also propose an algorithm to detect and quantify the shape collapse after image registration. By computing shape collapse map for each of 50 participants from a bipolar disorder study, we obtained a population shape-collapse probability map to evaluate percentage of the whole population that has a collapse problem at each point of the brain. By changing the size of smoothing kernel of the SyN algorithm, we show that we can reduce the shape collapse problem in our phantom example, but we still

have the poor correspondence problem. This study indicates that new methods are needed to reduce the shape collapse problem and improve the registration quality.

CHAPTER 2
ILLUSTRATION OF PROBLEMS IN LARGE DEFORMATION IMAGE REGISTRATION WITH SHAPE COLLAPSE

By definition, the goal of image registration to is to find the pointwise correspondences between a moving image and a target image. Therefore, a good registration method is necessary to give a transformation that well defines the pointwise correspondences between two coordinate systems. The shape collapse problem is common in large deformation image registration and may cause problems such as incorrect pointwise correspondence, incorrect automatic segmentation and loss functional signal. In this chapter, we will demonstrate and explain those problems caused by shape collapse using both real and phantom examples.

2.1 Shape Collapse in Registration of 3D MR Brain Images

We first use the example of registering two 3D MR brain images in Fig.1.1 to identify the problems caused by shape collapse. An MR brain image (Fig.2.1a) was registered to a common brain atlas (Fig.2.1c) using symmetric diffeomorphic registration algorithm. Landmarks F1 and F2 are in the cerebrospinal fluid (CSF) of the brain in the moving image, and the correspondences between landmarks in moving and target images are defined by the output transformation of SyN algorithm. It appears that there is a collapse problem at the point F2; as we can see in the deformed moving image Fig.2.1b, the sulcus containing F2 in the moving image collapsed to a thin set during registration because the target image does not have a structure

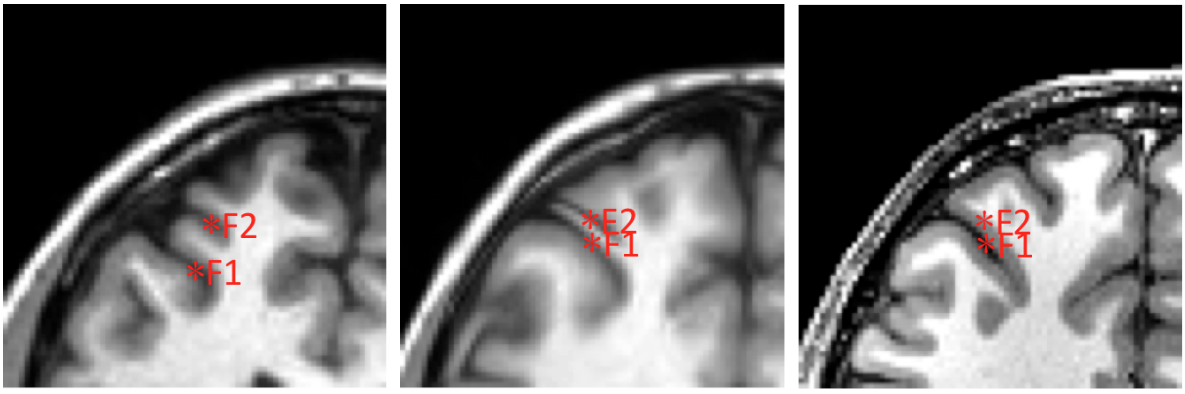

(a) Moving image with two landmarks

(b) Deformed moving with two transformed landmarks

(c) Reference image with two transformed landmarks

Figure 2.1: Demonstration of incorrect correspondence and loss of functional signal in regions with shape collapse.

similar to the sulcus containing F2 in the moving image. The point F1 in CSF of the moving image was mapped a point in CSF of the target image, but the point F2 in CSF of the moving image was mapped to a point in the gray matter of the target image, which is an incorrect point-to-point correspondence caused by shape collapse, i.e., the biological structure of the region containing F2 in the moving image does not correspond to the biological structure of F2 in the target image.

The example in Fig.2.1 also shows that shape collapse may lead to incorrect automatic image segmentation. Automatic image segmentation is to first register the moving image with the target image, and then deform the label map of the moving image into the target image space using the generated correspondence mapping to obtain a segmentation of the target image. Shape collapse may lead to incorrect auto-

matic image segmentation because it may cause incorrect pointwise correspondence.

Finally, the example in Fig.2.1 also demonstrates that shape collapse may also cause loss of functional signal. Suppose there are some functional signal in the gray matter around F2, since the sulcus collapsed to a really thin set during registration, we will lose the functional signal if we use the correspondence transformation to map the functional data to the target image space.

2.2 Shape Collapse in Registration of 2D Cortex Phantoms

We used the phantom example in Fig.1.2 to give an explicit demonstration of stated disadvantages of shape collapse in large deformation image registration. Figure 2.2 shows the results of registering a 2D moving cortex phantom image (Fig.2.2a) to a 2D target cortex phantom image (Fig.2.2b) using SyN diffeomorphic image registration algorithm. Notice that the final deformed image (Fig.1.2d) and the target image look very similar, but when we zoom in the region of the sulcus and overlay the moving image with segmentation of the sulcus (see colored regions in Fig.2.2c) and deform it into the target image space using the transformation from SyN algorithm. The deformed image with deformed segmentation overlaid (See Fig.2.2d) shows that the red region in the moving image collapsed to a thin set with almost zero volume in the target image space during registration, which may lead to loss of functional signal if there are some functional data near the red region and we map them into the target image space using the transformation with collapse.

In this example, we can also see that shape collapse causes incorrect pointwise

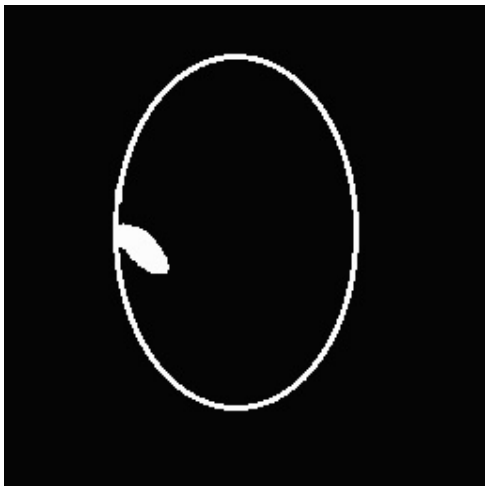

(a) Moving phantom image

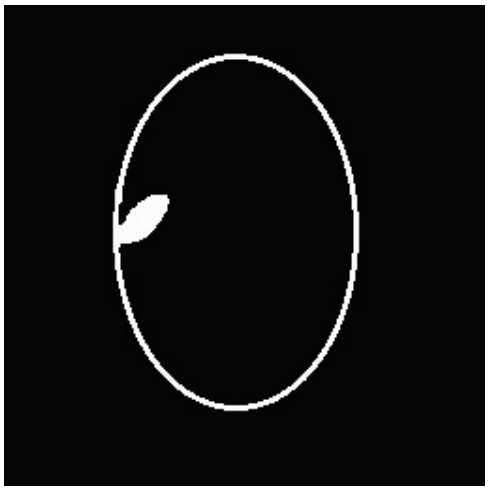

(b) Target phantom image

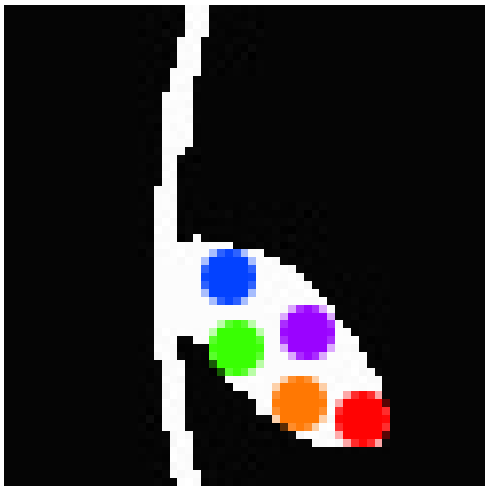

(c) Segmentation overlaid on moving image

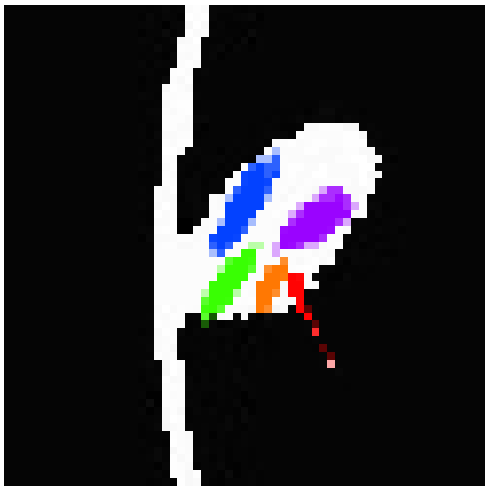

(d) Deformed moving image with deformed segmentation overlaid

Figure 2.2: A phantom example showing loss of functional data and incorrect correspondences when using SyN diffeomorphic image registration.

correspondence. For example, the tip of the sulcus (on the boundary of the red region) in the moving image was not mapped to the tip of sulcus in the target image space; and the colored circular regions in the moving image were mapped to oval-shaped regions in the target image. This phantom example also shows that shape collapse may cause incorrect automatic image segmentation. For example, if we obtain the segmentation of the target image by deforming the label map of the moving image into the target image space using the transformation with collapse, we end up with a bad segmentation of the sulcus in the target image because of incorrect correspondence problem.

CHAPTER 3
METHODS

3.1 SyN, Symmetric Diffeomorphic Image Registration

The SyN symmetric diffeomorphic image registration algorithm [1] registers two images by mapping each image to a midpoint coordinate system (See Fig.3.1). Let $I : \Omega \to \mathbb{R}$ and $J : \Omega \to \mathbb{R}$ represent two images to be registered where $\Omega \subset \mathbb{R}^n$ is the domain of the images. Define $\phi : \Omega \times [0,1] \to \Omega$ to be an isotopy between the functions $\phi(\cdot, 0) = f$ and $\phi(\cdot, 1) = g$ such that $f = Id$ is the identity map and g is the mapping that deforms I into the shape of J via the action $g \cdot I \triangleq I(g^{-1})$. Define $\psi : \Omega \times [0,1] \to \Omega$ similarly such that $\psi(\cdot, 0) = Id$ and $\psi(\cdot, 1) \cdot J = J(\psi^{-1}(\cdot, 1))$ maps J into the shape of I. Let $v : [0,1] \to V$ and $w : [0,1] \to V$ be time-dependent velocity vector fields (See Fig.3.2) where V is a Hilbert space of smooth, compactly supported vector fields on Ω. The diffeomorphic properties of the transformation ϕ and ψ comes from the fact that they are parametrized by the smooth velocity fields v and w through the O.D.E $\frac{d}{dt}\phi(x,t) = v(\phi(x,t),t)$ and O.D.E $\frac{d}{dt}\psi(x,t) = w(\psi(x,t),t)$, where $t \in [0,1]$, $x \in \Omega$, and the velocity fields $v, w \in L^2([0,1], V)$ [3]. We can interpret the above O.D.E used to parametrize ϕ as: The differential of the curve/path $\phi(x, \cdot)$ at time point t is a tangent vector at the point $\phi(x,t)$, which equals the value of the vector field $v(\cdot, t)$ at point $\phi(x,t)$.

The SyN registration algorithm is stated as: Minimize the following cost func-

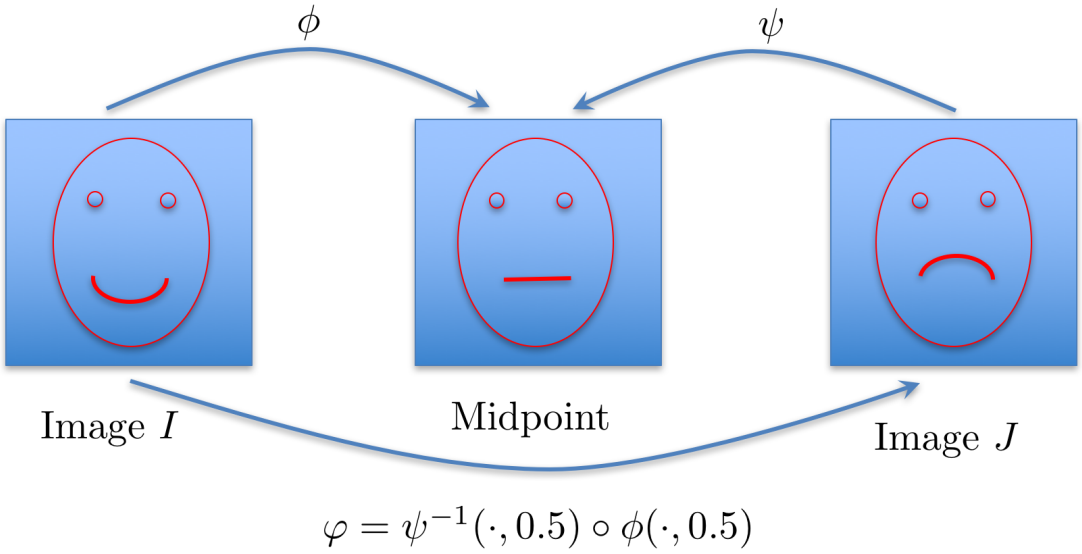

Figure 3.1: SyN algorithm registers two images in the midpoint coordinate system.

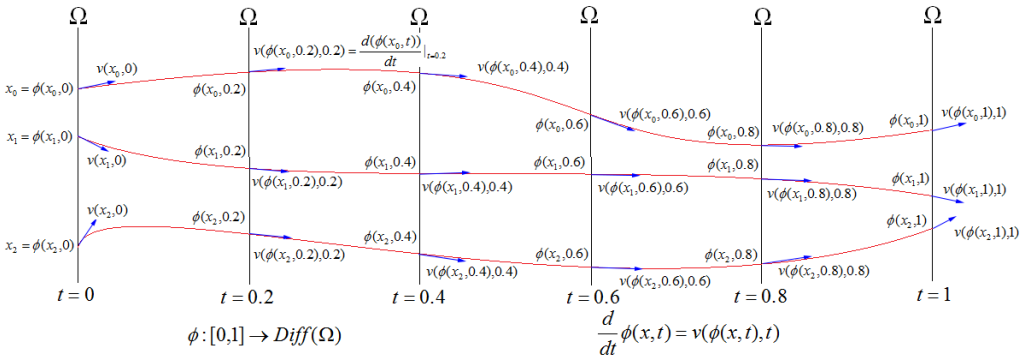

Figure 3.2: The flow diffeomorhism ϕ parametrized by the velocity field v.

tion with respect to velocity vector fields v and w

$$E(v,w) = \int_0^{0.5} \Big\{ ||v(x,t)||_V^2 + ||w(x,t)||_V^2 \Big\} dt + \int_\Omega CC\big(I(\phi^{-1}(x,0.5)), J(\psi^{-1}(x,0.5))\big) dx \tag{3.1}$$

where the first term is the regularization term used to evaluate the smoothness of the velocity vector fields v and w, $||\cdot||_V$ is a Sobolev norm on vector fields in the domain Ω; the second term is the normalized cross correlation between the two deformed images.

Notice that the normalized cross correlation is computed in a midpoint coordinate system that is half-way between the coordinate systems of I and J, i.e., in the $t = 0.5$ coordinate system.

Following the notation of [1], the normalized cross correlation is defined in the following way. Define the images with their local mean subtracted as $\bar{I}(x) = I(\phi_0^{-1}(x,0.5)) - \mu_I(x)$ and $\bar{J}(x) = J(\phi_1^{-1}(x,0.5)) - \mu_J(x)$ where μ_I and μ_J are the the local intensity means of the voxels centered at x in a $N \times N \times N$ window of deformed images I and J, respectively. We usually choose N to be 5. The normalized cross correlation between two deformed images at point x (in the midpoint coordinate system) is then defined as

$$CC(\bar{I}, \bar{J}) = \frac{< \bar{I}, \bar{J} >^2}{< \bar{I} >< \bar{J} >} = \frac{A^2}{BC} \tag{3.2}$$

where the inner products are taken over a $N \times N \times N$ window.

The inner-product of two vector fields in the vector space V is defined through

a differential operator L given by:

$$< f, g >_V \triangleq < Lf, Lg >_{L^2} = < L^+ Lf, g >_{L^2} \tag{3.3}$$

where L^+ is the adjoint of operator L.

From the above construction of the vector space V, a compact self-adjoint operator [3] $K : L^2(\Omega, \mathbb{R}) \to V$ is uniquely defined by

$$< a, b >_{L^2} = < Ka, b >_V \tag{3.4}$$

The operator K is a Gaussian filter in the implementation of SyN algorithm in ITK, i.e. $K(x) = \frac{1}{\sqrt{2\pi}\sigma} e^{-|x|^2/\sigma^2}$.

Let $\phi_{s,t} : \Omega \to \Omega$ denote the composition $\phi_{s,t} = \phi_t \circ (\phi_s)^{-1}$. The interpretation of $\phi_{s,t}(y)$ is that it is the position at time t of a particle that started at position y at time s [3].

Lemma 3.1.1. *The variation of mapping $\phi_{s,t}$ when $v \in L^2([0,1], V)$ is perturbed along $h \in L^2([0,1], V)$ is given by [3]:*

$$\begin{aligned} \delta_h \phi^v_{s,t} &= \lim_{\epsilon \to 0} \frac{\phi^{v+\epsilon h}_{s,t} - \phi^v_{s,t}}{\epsilon} \\ &= \frac{d\phi^{v+\epsilon h}_{s,t}}{d\epsilon}|_{\epsilon=0} \\ &= D\phi^v_{s,t} \int_s^t (D\phi^v_{s,u})^{-1} h_u \circ \phi^v_{s,u} du \end{aligned} \tag{3.5}$$

Proof. The curve $\phi^v : [0,1] \to Diff(\Omega)$ is defined via the evolution equation

$$\frac{d}{dt}\phi^v_t(x) = v_t(\phi^v_t(x)) \tag{3.6}$$

The superscript v in ϕ^v is used to to denote explicit dependence of ϕ on the velocity

field v. We first show the following two equations are true:

$$\begin{aligned}
\frac{d\phi_{s,t}^{v+\epsilon h}}{dt} &= \frac{d(\phi_t^{v+\epsilon h} \circ (\phi_s^{v+\epsilon h})^{-1})}{dt} && \text{By definition} \\
&= (v_t + \epsilon h_t)\Big(\phi_t^{v+\epsilon h}\big((\phi_s^{v+\epsilon h})^{-1}\big)\Big) && \text{(Using Eq.3.6)} \\
&= v_t \circ \phi_t^{v+\epsilon h} \circ (\phi_s^{v+\epsilon h})^{-1} + \epsilon h_t \circ \phi_t^{v+\epsilon h} \circ (\phi_s^{v+\epsilon h})^{-1} \\
&= v_t \circ \phi_{s,t}^{v+\epsilon h} + \epsilon h_t \circ \phi_{s,t}^{v+\epsilon h} && \text{By definition}
\end{aligned} \tag{3.7}$$

We have an additional result given by:

$$\frac{d}{dt} D\phi_{s,t}^v = D\frac{d}{dt}\phi_{s,t}^v = D(v_t \circ \phi_{s,t}^v) = D_{\phi_{s,t}^v} v_t D\phi_{s,t}^v \tag{3.8}$$

The first equality in Eq. 3.8 follows from the commutativity of partial derivatives. The second equality follows from substituting Eq. 3.6 for $\frac{d}{dt}\phi_{s,t}^v$. The last equality follows from the chain rule. Note that the following notations are equivalent: $D_{\phi_{s,t}^v} v_t = (Dv_t) \circ \phi_{s,t}^v = (Dv_t)|_{\phi_{s,t}^v}$, i.e., this notation refers to the differential of v_t evaluated at $\phi_{s,t}^v$.

Computing the differential of the left-hand side of Eq.3.5 in ϵ at $\epsilon = 0$ gives

$$\begin{aligned}
\frac{d}{dt}\delta_h\phi_{s,t}^v &= \frac{d}{dt}\Big(\frac{d\phi_{s,t}^{v+\epsilon h}}{d\epsilon}|_{\epsilon=0}\Big) \\
&= \frac{d}{d\epsilon}\Big(\frac{d\phi_{s,t}^{v+\epsilon h}}{dt}\Big)|_{\epsilon=0} \\
&= \frac{d}{d\epsilon}\Big(v_t \circ \phi_{s,t}^{v+\epsilon h} + \epsilon h_t \circ \phi_{s,t}^{v+\epsilon h}\Big)|_{\epsilon=0} && \text{(Using Eq.3.7)} \\
&= \Big((Dv_t \circ \phi_{s,t}^{v+\epsilon h})\frac{d\phi_{s,t}^{v+\epsilon h}}{d\epsilon} + h_t \circ \phi_{s,t}^{v+\epsilon h} + \epsilon\frac{d}{d\epsilon}(h_t \circ \phi_{s,t}^{v+\epsilon h})\Big)|_{\epsilon=0} \\
&= (D_{\phi_{s,t}^v} v_t)\delta_h\phi_{s,t}^v + h_t \circ \phi_{s,t}^v
\end{aligned} \tag{3.9}$$

with initial condition $\delta_h\phi_{s,s}^v = 0$ since $\phi_{s,s}^v$ is an identity map for any velocity field v.

Let $y(t) = \delta_h \phi^v_{s,t}$, $p(t) = -D_{\phi^v_{s,t}} v_t$ and $q(t) = h_t \circ \phi^v_{s,t}$. Then Eq.3.9 can be written as

$$\frac{dy}{dt} + p(t)y = q(t) \tag{3.10}$$

The general solution to the linear first order differential equation in Eq.3.10 is given by [18]

$$y = Ce^{-\int_s^t p(w)dw} + e^{-\int_s^t p(w)dw} \times \int_s^t q(u) e^{\int_s^u p(w)dw} du \tag{3.11}$$

Notice that $e^{-\int_s^t p(w)dw} x(s)$ is the solution to the following O.D.E: $\dot{x}(t) = -p(t)x(t)$ with initial condition $x(s)$. According to Eq.3.8, we know that $e^{-\int_s^t p(w)dw} x(s) = x(t) = D\phi^v_{s,t}$. Substitute t with s, we have $e^{-\int_s^s p(w)dw} x(s) = x(s) = D\phi^v_{s,s} = \mathbb{1}$ since $\phi^v_{s,s}$ is the identity map whose differential is the identity matrix. Thus $e^{-\int_s^t p(w)dw} = D\phi^v_{s,t}$. Also notice that $e^{\int_s^u p(w)dw} = (e^{-\int_s^u p(w)dw})^{-1} = (D\phi^v_{s,u})^{-1}$. Then Eq.3.11 can be rewritten as

$$y = CD\phi^v_{s,t} + D\phi^v_{s,t} \times \int_s^t q(u) \times (D\phi^v_{s,u})^{-1} du \tag{3.12}$$

Using the initial condition $y(s) = \delta_h \phi^v_{s,s} = 0$, we know the constant C in Eq.3.12 is euqal to 0. Thus, we have

$$\begin{aligned} \delta_h \phi^v_{s,t} = y(t) &= D\phi^v_{s,t} \times \int_s^t q(u) \times (D\phi^v_{s,t})^{-1} du \\ &= D\phi^v_{s,t} \times \int_s^t h_u \circ \phi^v_{s,u} \times (D\phi^v_{s,u})^{-1} du \end{aligned} \tag{3.13}$$

This is exactly the same as Eq.3.5.

Using lemma 3.1.1 and following the derivations in Beg et al. [3] and Avants et al. [1], the gradients of the energy functional with respect to $v(t)$ and $w(t)$ are given by

$$\nabla_v E = 2v(x,t) + K\left(\frac{2A}{BC} \times \left(\bar{J}(x) - \frac{A}{B}\bar{I}(x)\right) |D\phi^{-1}(x, 0.5)| \nabla \bar{I}(x)\right) \tag{3.14}$$

$$\nabla_w E = 2w(x,t) + K\left(\frac{2A}{BC} \times \left(\bar{I}(x) - \frac{A}{C}\bar{J}(x)\right)|D\psi^{-1}(x,0.5)|\nabla\bar{J}(x)\right) \tag{3.15}$$

3.2 Diffeomorphic Demons Registration

Thirion's demons algorithm considers deformable image registration as a diffusion process [20]. To match two images, demons algorithm considers the boundary of an object O in one image S (called a scene image) as semi-permeable membranes and the other image M (called a model image), considered as a deformable grid, is deformed by effectors inside the membranes [20]. In [20], a demon at a point $p \in S$ is defined to be an effector which acts locally to push (if the corresponding point $p' \in M$ is inside O) or pull (if the corresponding point $p' \in M$ is outside O) the model image M. There is an associated elementary force for each demon, and the set of all demons forces can be used to update the transformation from model image M to scene image S.

Vercauteren el at. [21] extended Thirion's demons algorithm to a non-parametric diffeomorphic image registration algorithm, diffeomorphic demons algorithm, to obtain smoother and more accurate transformations. Given two images $M : \Omega \to \mathbb{R}$ and $F : \Omega \to \mathbb{R}$, and a diffeomorphic transformation $s \in Diff(\Omega)$, the diffeomorphic demons algorithm aims to find stationary velocity field u that minimizes the following correspondence energy:

$$E_s^{corr}(u) = ||F - M \circ s \circ exp(u)||^2 + \frac{1}{\sigma^2} dist(s, s \circ exp(u))^2 \tag{3.16}$$

where the distance function $dist$ between two diffeomorphisms $s, c \in Diff(\Omega))$ is given by $dist(s,c) = ||Id - s^{-1} \circ c||$. The diffeomorphic demons algorithm is stated

as follows [21]:

1. Given the current transformation $s \in Diff(\Omega)$, compute an update field u by minimizing $E_s^{corr}(u)$ in Eq.3.16 with respect to u.
2. Let $c \leftarrow s \circ exp(u)$.
3. Let $s \leftarrow K \star c$, where K is a Gaussian kernel.

In some cases, for example registration of MR brain images, diffeomorphic demons registration algorithm can achieve similar results to registration algorithms whose transformations are parametrized by time-variant velocity fields [10].

3.3 Collapse Detection Algorithm

Figure 3.3 shows collapse of an oval-shaped region (region inside the red oval in the moving image), which contains cortex that has a collapse problem in the example of registration of two MR images (See Fig.1.1) into a thin set (region inside the red oval) in the target image space. Figure 3.4 is an animation showing the collapse of a simple oval into a thin segment (from panel a to panel d), where blue arrows show the direction of collapse.

To deform an image, we use the pullback transformation, the red arrows in Fig.3.5 starting from the thin segment shows the pullback transformation. The transformation ϕ acting on image I is defined to be $I \circ \phi^{-1}$, notice ϕ^{-1} is the pullback transformation defined in the target image space. The yellow point (in the target image space) in the thin segment has a shape collapse problem; Regions inside the yellow circle is a small neighborhood of it. Points in this neighborhood at the base

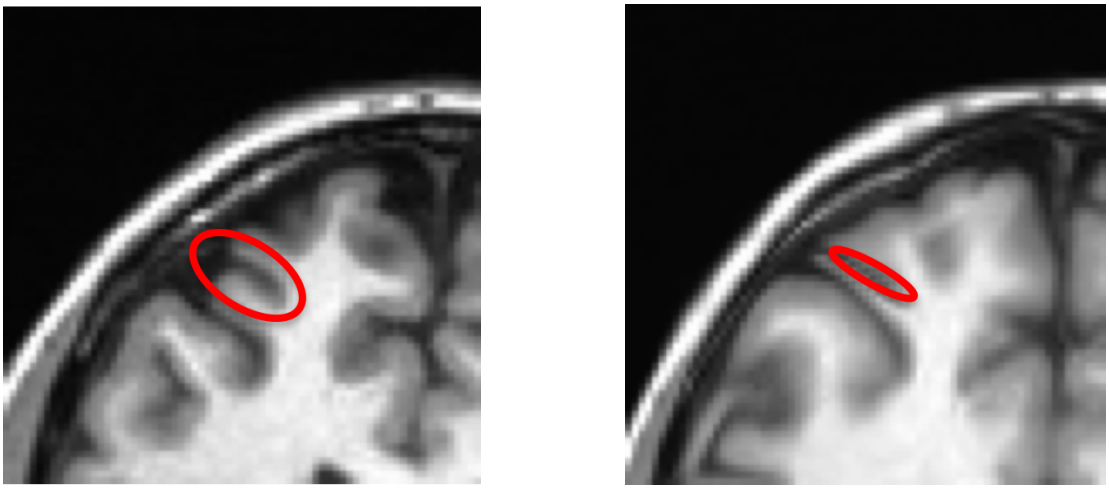

(a) An oval region in the moving image within which there is a collapse

(b) Oval region collapsed to a thin set

Figure 3.3: Collapse of a oval region in the moving MR image.

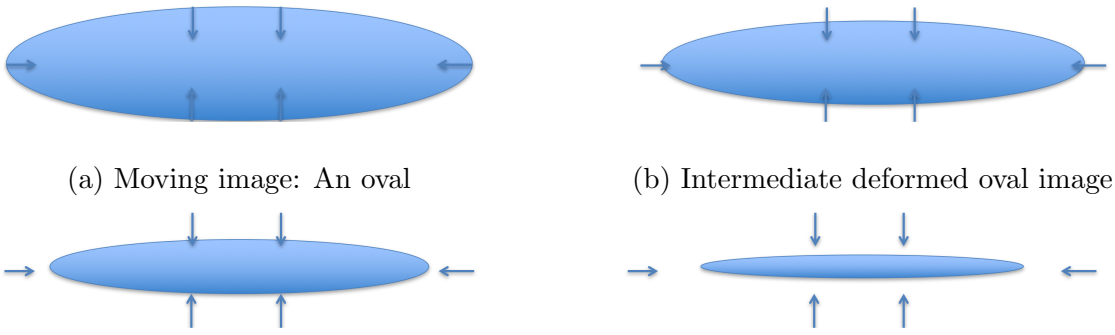

(a) Moving image: An oval

(b) Intermediate deformed oval image

(c) Intermediate deformed oval image

(d) Final deformed oval image

Figure 3.4: An animation showing collapse of a simple oval region into a thin segment.

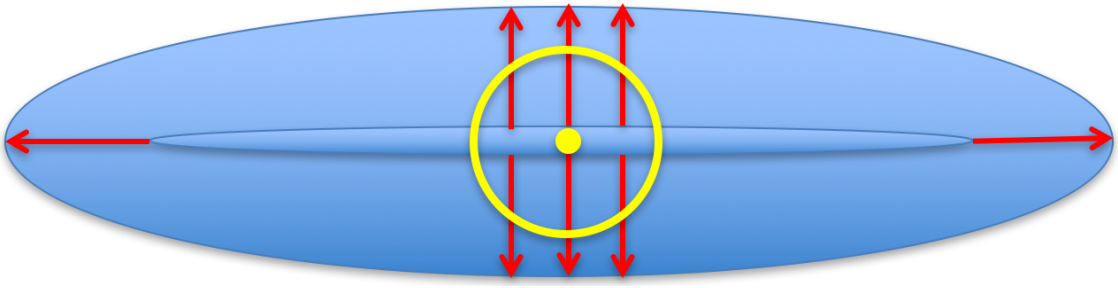

Figure 3.5: Pullback transformation. Points inside the yellow circle, which is a neighborhood of a yellow point that has a collapse problem, come from different regions in the moving image defined by the pullback transformation.

of top arrows come from the top of the big oval and points at the base of the bottom arrows come from the bottom of the big oval; those points in the big oval forms several almost disjoint sets.

Using pullback transformation, we introduce our idea of collapse detection in 2D case. Given a point in the target image space, we look at the displacement vectors in a 3 by 3 neighborhood about it (Fig.3.6a), and move the vectors to the same starting point (Fig.3.6b). If there is a shape collapse at that point, the points in the neighborhood of it will move in the opposite directions by the pullback transformation, thus we can separate them into two or more clusters in the moving image space. If there is no shape collapse, the points move in almost the same direction (See Fig.3.7). We used the k-means clustering algorithm to define the center of each cluster, and compute the distance between the cluster centers to define the amount of shape collapse at a point p.

Now we state our collapse detection algorithm in a more rigorous way. Let Ω_0 and Ω_1 be two differentiable manifolds that represent the domains of images $I : \Omega_0 \to \mathbb{R}$ and $J : \Omega_1 \to \mathbb{R}$, respectively. Define the transformation $\varphi : \Omega_0 \to \Omega_1$ to be the transformation that acts on I_0 to transform it into the shape of I_1 via the action $\varphi \cdot I_0 \triangleq I_0(\varphi^{-1})$. Note that $\varphi^{-1} : \Omega_1 \to \Omega_0$ is a mapping from the domain of I_1 to the domain of I_0. We say that a collapse happens at $y \in \Omega_0$ when φ maps an open set $U \subset \Omega_0$ containing y to an open set $\varphi(U) \subset \Omega_1$ of near zero measure. Alternatively, we say a collapse happens at $x \in \Omega_1$ if there exists an open (round) ball $V \in \Omega_1$ containing x such that $\varphi^{-1}(V)$ is mapped to an almost disconnected set (concentrated in at least two different regions joined by thin connectors, such as an hourglass) in Ω_0.

Theoretically, shape collapse occurs in regions of near Jacobian determinant with respect to the push forward transformation φ. But in practice, we do not use Jacobian determinant as a measure of shape collapse for the following reasons: (1) To compute the Jacobian of a large deformation, we need all the intermediate transformations, and it requires a lot of calculations; (2) We cannot just use the final transformation to calculate the Jacobian because the displacement vectors of a large deformation may cross each other and give negative Jacobian determinants; (3) We do not always have access to the intermediate transformations; (4) The Jacobian determinant at each point is a scalar, it can not tell us the direction of shape collapse but our collapse detection algorithm can.

The second definition of shape collapse above is more convenient for detecting

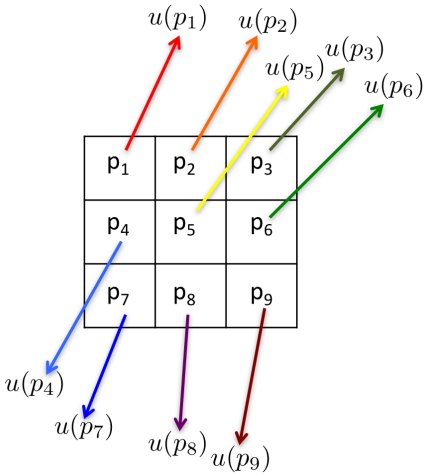

(a) Displacement vectors at a point with collapse

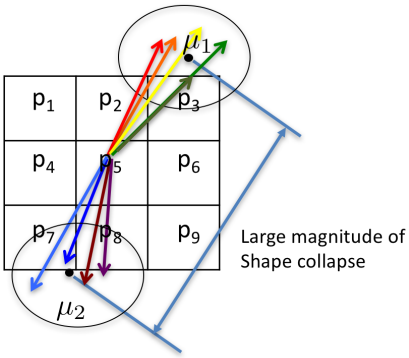

(b) Centered displacement vectors at a point with collapse

Figure 3.6: With shape collapse, points pullback from at least two disjoint regions in the moving image.

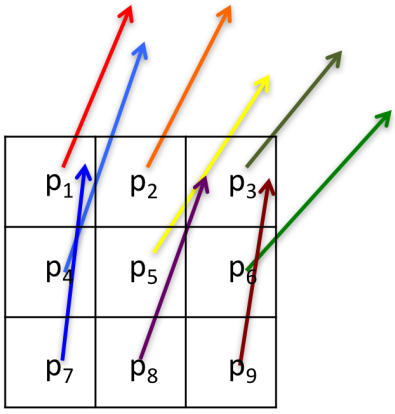

(a) Displacement vectors at a point with collapse

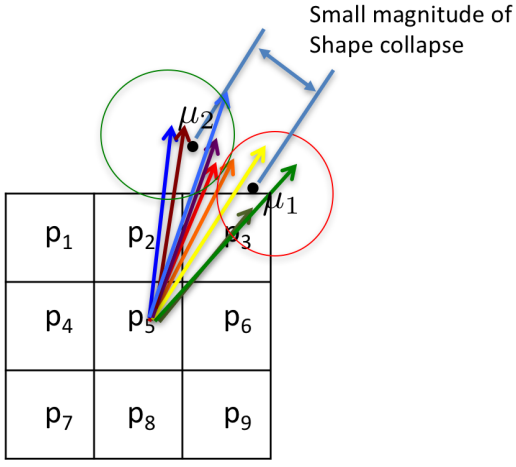

(b) Centered displacement vectors at a point with collapse

Figure 3.7: Without shape collapse, points pullback from a single connected region in the moving image.

points of collapse in image registration since φ^{-1} is used to compute the deformed image of I_0 into the shape of I_1. In the case of the SyN registration algorithm, we define $\varphi^{-1} \triangleq \phi^{-1}(\cdot, 0.5) \circ \psi(\cdot, 0.5)$ and $\Omega_0 = \Omega_1 = \Omega$ to be consistent with Eq. 3.1.

The following algorithm is used to detect where points of collapse occur in the domain Ω_1 of the image I_1. Let $G_1 \subset \Omega_1$ denote the discrete collection of voxel center locations corresponding to the centers of the voxels of image I_1. Repeat the following steps for each $x \in G_1$.

1. Let $N_x \subset G_1$ be a neighborhood of x.
2. Let $D_x = \{\varphi^{-1}(y) - y | y \in N_x\}$ be the set of displacement vectors in the neighborhood of x.
3. Compute the 2-means clustering of the set D_x. Let μ_1 and μ_2 denote the values of the two means, respectively.
4. Let $d_x = ||\mu_1 - \mu_2||$ denote the Euclidean distance between the two means.

Form the image of collapse points $C : \Omega_1 \to \mathbb{R}$ using the rule $C(x) = d_x$ for $x \in G_1$.

The results in this paper used a 3×3 voxel neighborhood for the 2D results and a $3 \times 3 \times 3$ voxel neighborhood for the 3D results.

CHAPTER 4
EXPERIMENTS AND RESULTS

4.1 Imaging Data

Anatomical images from a study of bipolar disorder were used in this analysis including images from 25 participants with bipolar disorder (14 male: 11 female; age m = 38.6, sd = 13.06) and 25 healthy control participants (14 male: 11 female; age m = 38.36, sd = 13.23). Participants provided written informed consent prior to participation in the study. T1-weighted images were acquired with $1mm^3$ isotropic resolution using a 3T Siemens scanner. T1-weighted images were acquired using a 3D magnetization-prepared rapid gradient echo sequence in the coronal plane (FOV: $256 \times 256 \times 256$ mm^3; matrix = $256 \times 256 \times 256$, TR=2530ms; TE = 2.3ms; TI = 909ms; flip angle = 10; bandwidth = 180 Hz/pixel; and R=2 GRAPPA).

4.2 Image Registration Using BRAINS AutoWorkup

BRAINS AutoWorkup [13] provides a framework for automatically analyzing MRI scans that incorporates several steps to provide well defined mappings between each subject scan and a common brain atlas (NAC HNCMA Atlas 2013 [9]). First, the anterior commissure (AC) point, posterior commissure (PC) point and 49 other fiducial points are automatically detected by the BRAINS Constellation Detector [8] for both the atlas and the subject images. A rigid transformation for each data set is computed that aligns the AC point to (0,0,0) and sets the PC point to (0,−|AC-PC|,0), and the mid-sagittal plane (MSP) is identified by optimizing the plane that

maximally correlates intensity values from the right hemisphere to the left hemisphere (as if reflected in a mirror). The rigid transformation is incorporated into the physical space definition of image headers to avoid introducing interpolation errors. This results in both the atlas and the subject being aligned at the AC point, along the AC-PC line, and within the MSP. Subsequent to this initialization phase, the previously identified 51 landmark points in atlas and subject space are used to estimate an affine transform used to initialize the symmetric diffeomorphic image registration. In this work, we use the inverse transformation estimated from BAW to register T1 AC-PC aligned image to the common atlas space.

4.3 Shape Collapse Measurement Results

By computing the Euclidean distance d_x, which represents the distance between means of two clusters defined by 2-mean clustering algorithm, for each point x in the atlas space, we can generate a shape collapse map for each participant after image registration. Figure 4.1 is a shape collapse map for one of the 50 participants. In this example, we used a color overlay to visualize the amount of shape collapse in different areas of the target image (Fig.4.1b). Red regions in the collapse map have more collapse during image registration. The regions with shape collapse are consistent with the areas where shape collapse were visually apparent in the deformed image (Fig.4.1a), confirming that our algorithm has successfully quantized the amount of shape collapse, and detected regions where shape collapse occurred during image registration.

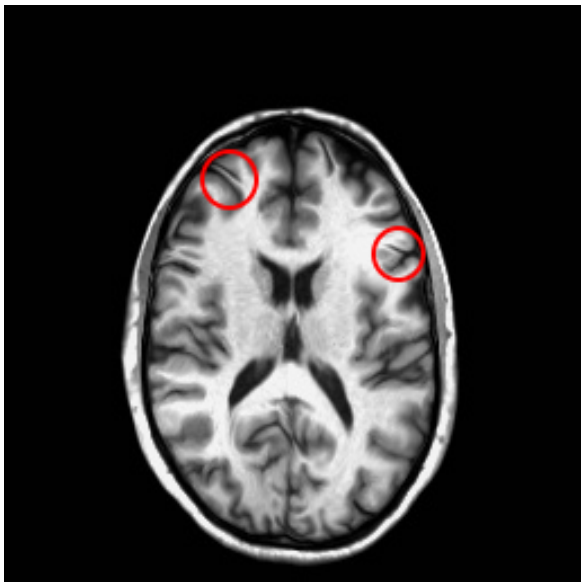

(a) Deformed T1 image

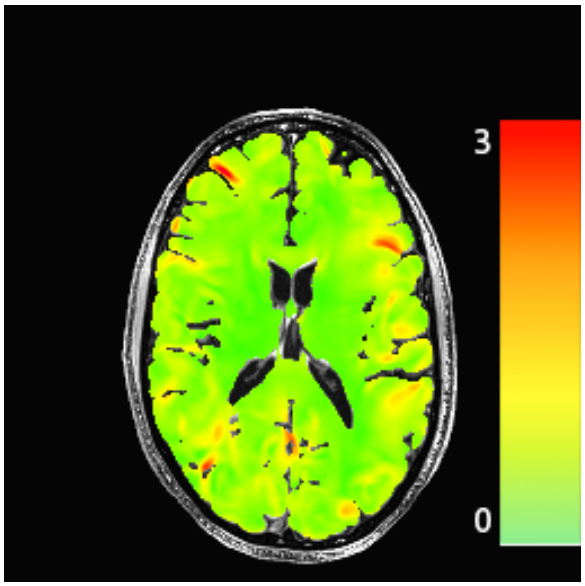

(b) Collapse measurement

Figure 4.1: Shape collapse detection for one participant. (a) same deformed image as in Fig. 1.1c; (b) color coded collapse image superimposed on image shown in (a) where green corresponds to a collapse value of 0 mm and to red corresponds to a collapse value of 3 mm. Red regions are regions with shape collapse after registration.

4.4 Population Shape-Collapse Probability Map

For neurological studies, many brain images of a whole population are mapped to a common atlas through pairwise registration. And each pairwise registration can potentially have shape collapse problem, we want to evaluate the percentage of the whole population that has a shape collapse problem at each point in the target image space. All these lead to the concept of population shape collapse probability map, which is explained in the rest of this section.

The shape collapse measurement/detection algorithm was used to compute the shape collapse map for each of the 50 participants (25 healthy controls and 25 people with bipolar disorder). A universal threshold T was applied to each of 50 shape collapse maps, then the average of all the 50 thresholded maps gives a population shape-collapse probability map for the whole brain. Let $C_i : \Omega \to \mathbb{R}$ denote the map of shape collapse measurement for the ith subject, where Ω is the domain of the target image. Let $Prob : \Omega \to \mathbb{R}$ denote the population shape collapse probability map of the population, for any point $p \in \Omega$ we have

$$Prob(p) = \frac{1}{50} \sum_{i=1}^{50} Thres(C_i(p))) \tag{4.1}$$

where $Thres : \mathbb{R} \to \{0, 1\}$ is a function defined as $Thres(a) = 0$ if $a < T$, and $Thres(a) = 1$ if $a \geq T$. Choice of the threshold function is our choice of the definition of whether there is a shape collapse problem at a point or not, i.e. if $C_i(p) < T$ then there is no collapse problem at point p of the ith participant, otherwise, there is a collapse problem at point p of the iith participant during registration. The population shape collapse probability map of 50 subjects is shown in Fig.4.2, which was obtained

with threshold value $T = 1$ (i.e., the threshold value of the $Thres$ function in Eq. 4.1 was set to 1). This color-coded population, shape-collapse, probability maps was thresholded at 0.6 (i.e. regions with value less than 0.6 are not visualized). Regions of red and orange show areas where collapse occurs for at least 60% of the individuals in the population.

The population, shape-collapse, probability map gives information about the regions where shape collapse problem is more likely to occur for this population during diffeomorphic image registration. This information can be used to determine whether or not there is functional signal loss when mapping functional data to a reference coordinate system, develop algorithmic solutions to reduce shape collapse problems and to determine the validity of population shape measurements when using nonrigid image registration methods.

4.5 Gaussian Smoothing Kernel Analysis

We investigated the influence of the Gaussian smoothing kernel K (see Eq. 3.4) in the SyN registration algorithm on reducing shape collapse using the 2D moving and target phantom images shown in Fig. 1.2. The SyN registration algorithm was used to register the moving brain phantom to the target brain phantom using a Gaussian smoothing kernel with different variances σ^2. Results of these experiments are shown in Fig. 4.3. As we can see from the collapse maps, the collapse problem is reduced while increasing the Gaussian kernel size. To see how well the transformations for different Gaussian kernel size are, we overlaid the moving image with segmentation

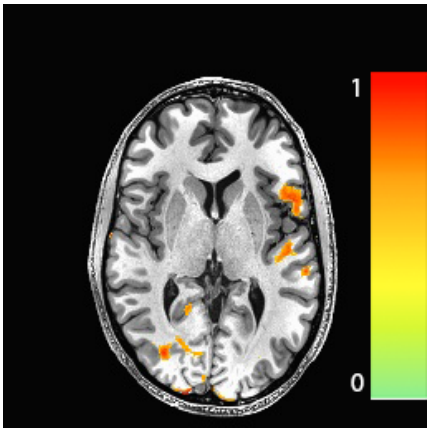

(a) Axial view

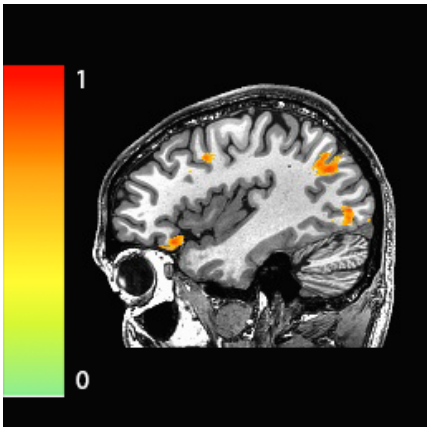

(b) Sagittal view

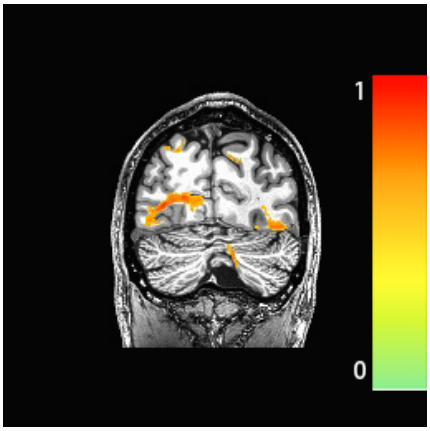

(c) coronal view

Figure 4.2: Orthogonal views of the 3D population, shape-collapse, probability map in the atlas space (includes 25 normal controls and 25 euthymic individuals).

(a) Deformed image, $\sigma^2 = 1$

(b) Deformed image, $\sigma^2 = 1.5$

(c) Deformed image, $\sigma^2 = 2$

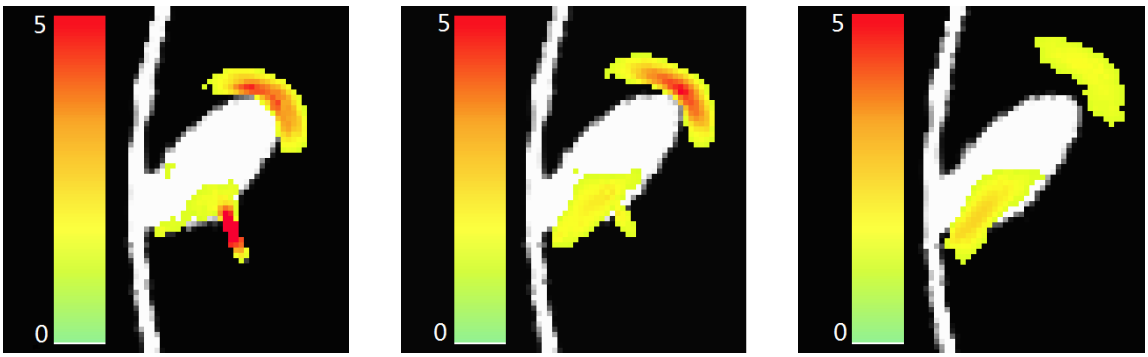

(d) Collapse map, $\sigma^2 = 1$

(e) Collapse map, $\sigma^2 = 1.5$

(f) Collapse map, $\sigma^2 = 2$

Figure 4.3: Registration results for three SyN registrations that registered the moving and target images shown in Fig. 1.2. The variance σ^2 of the Gaussian smoothing kernel used for registration is shown under each panel. Each collapse map was thresholded at a value of 2.0 mm for better visualization. Notice that more collapse happens when using Gaussian kernel with a smaller variance than with a larger variance.

and deform it with the transformation generated by the SyN algorithm. Although the collapse reduced as we increase the size of the Gaussian kernel, we still have poor

pointwise correspondence problem. For example, tip of the sulcus in the moving image was not mapped to the tip of sulcus in the target image as we increase the kernel size. Another example, circular regions are still distorted to oval shaped regions. In this example, we can say that reducing collapse by increasing variance of Gaussian filter does not mean we have solved the incorrect correspondence problem.

Table 4.1 shows the cross correlation and sum of squared differences between the deformed moving image and the target image for different sizes of Gaussian smoothing kernel. This table shows that as we increase the variance of Gaussian kernel, the shape collapse problem is reduced and the registration result is getting better. But when the variance becomes too large (i.e., variance = 3), although the shape collapse still goes down, the registration result is getting worse. Therefore, this is a trade off between the amount of collapse we want to reduce and the performance of registration algorithm in terms of similarity between the deformed moving image and the target image.

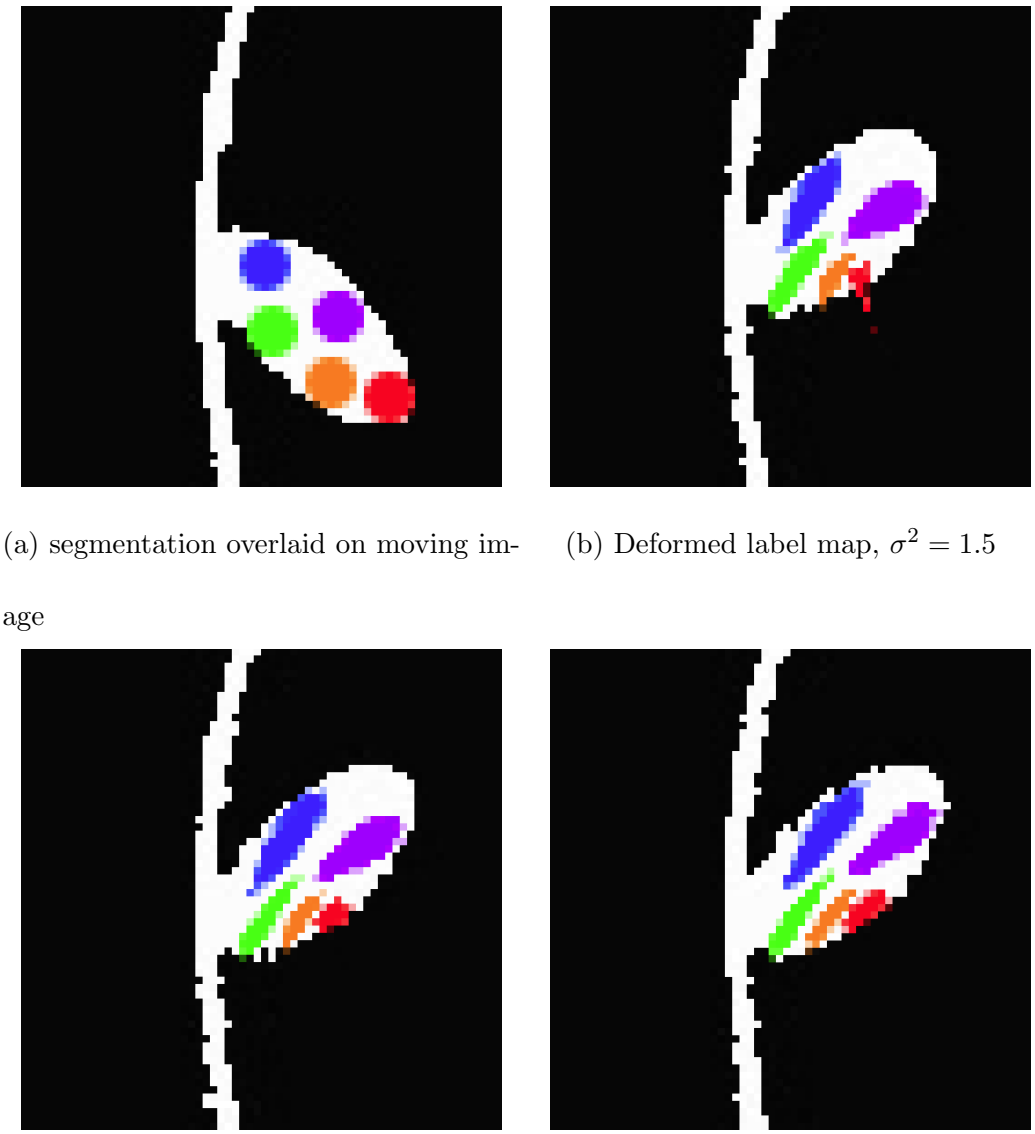

(a) segmentation overlaid on moving image

(b) Deformed label map, $\sigma^2 = 1.5$

(c) Deformed label map, $\sigma^2 = 2$

(d) Deformed label map, $\sigma^2 = 4$

Figure 4.4: Deformed segmentation image with different Gaussian kernel size.

Variance, σ^2	Collapse$_{mean}$	Collapse$_{max}$	CC	Sqrt(SSD)
1.5	1.71	6.24	0.9900	1544
2	1.66	4.90	0.9945	1152
2.5	1.58	3.01	0.9931	1293
3	1.55	3.17	0.9942	1180
3.5	1.54	3.06	0.9936	1245
4	1.53	2.97	0.9894	1606
6	1.50	3.10	0.9894	1596
9	1.44	2.85	0.9825	2049

Table 4.1: Results of SyN registration with different smoothing kernels. The first column shows the different smoothing variances used for the Gaussian smoothing kernel. The second and third columns show the mean and maximum values of voxels with value greater than 1 mm in the collapse map, respectively. The last column shows the square roots of the sum of squared differences between the deformed moving image and target image.

4.6 Shape Collapse Problem in Diffeomorphic Demons Algorithm

We have been using the symmetric diffeomorphic registration algorithm as a representative to examine shape collapse problem in large deformation image registration methods. The SyN algorithm uses time-variant velocity field to parametrize the flow of diffeomorphisms while diffeomorphic demons algorithm uses stationary velocity field. Although diffeomorphic demons algorithm has less degrees of freedom than SyN algorithm, we show that shape collapse problem also exists in diffeomorphic demons algorithm using the above cortex phantom example.

Figure 4.5 shows how one cortex in Fig.4.5a collapsed to match another cortex

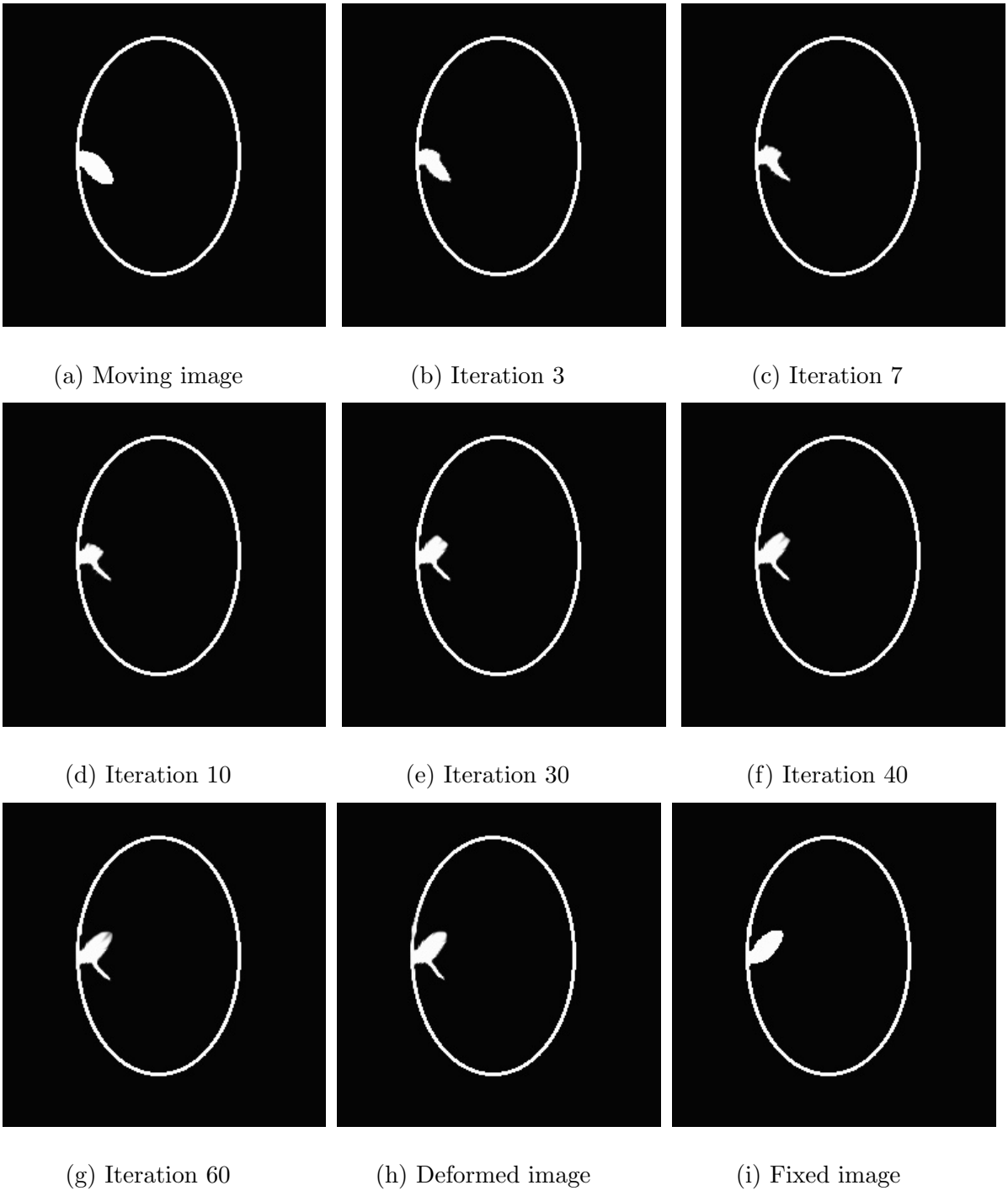

(a) Moving image (b) Iteration 3 (c) Iteration 7

(d) Iteration 10 (e) Iteration 30 (f) Iteration 40

(g) Iteration 60 (h) Deformed image (i) Fixed image

Figure 4.5: Process of the collapse of phantom cortex using diffeomorphic demons.

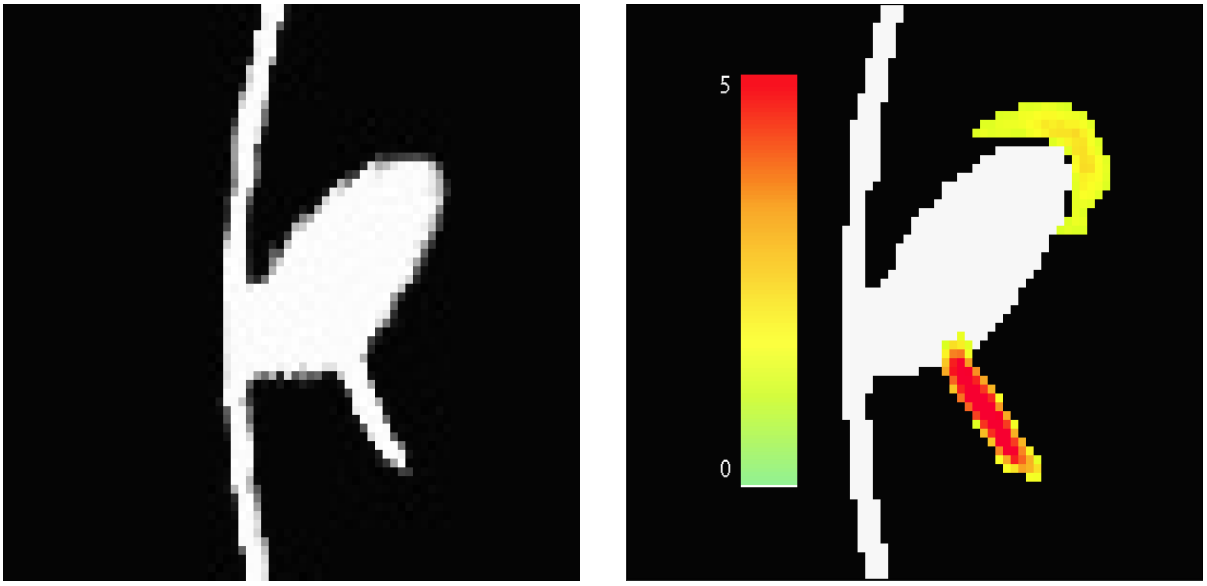

(a) Deformed image (b) Collapse map

Figure 4.6: Collapse map of diffeomorphic demons registration.

in Fig.4.5i when using diffeomorphic demons registration algorithm. The way how cortex collapsed in Fig.4.5 during diffeomorphic demons registration is similar to collapse of cortex in Fig.1.3 during SyN diffeomorphic registration, i.e., cortex collapsed on the bottom and a new cortex grew out from the top.

In figure 4.6, which shows the collapse map of diffeomorphic demons registration, we can see that a large amount of collapse occurred at the bottom of the cortex and some collapse (collapse of the background) also occurred at the top of the cortex. This is consistent with the collapse process of cortex shown in Fig.4.5.

In figure 4.7, we deformed the moving image with segmentation overlaid (Fig.4.7a) using the transformation from diffeomorphic demons registration output. The deformed label map (Fig.4.7b) also demonstrates that collapse problem causes: (1)

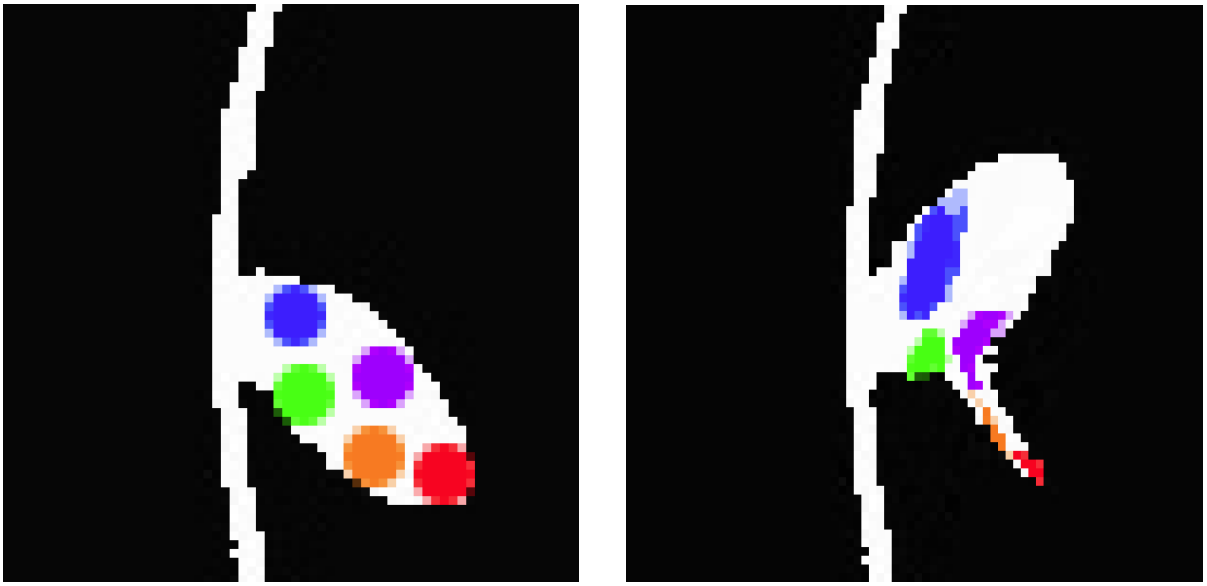

(a) Moving image with segmentation overlaid

(b) Deformed moving image with deformed segmentation overlaid

Figure 4.7: Collapse problem in diffeomorphic demons registration leads to incorrect correspondence and loss of functional signal.

incorrect pointwise correspondence, e.g., the red and orange regions in the moving image were not mapped to the corresponding regions in the fixed image; (2) loss of functional signal, suppose there are some functional data inside the red and orange regions, if we use this transformation to map the functional data to fixed image space, we will lose lots of functional data because of collapse.

CHAPTER 5
CONCLUSION AND DISCUSSION

Shape collapse occurs in image registration when a region in the moving image is transformed into a set of near measure zero. We introduced a new method to detect shape collapse in pairwise nonrigid image registration and demonstrated that shape collapse problem exists in large deformation image registration methods by using the symmetric diffeomorphic registration algorithm and the diffeomorphic demons registration algorithm as representatives. We showed that we need to consider shape collapse problem seriously because it may lead to incorrect pointwise correspondence, which consequently causes incorrect automatic image segmentation, and shape collapse may also results in loss of functional data when we map all functional data into a common space using a transformation with shape collapse.

We extended our shape collapse detection algorithm to compute the population, shape-collapse probability map. This map can be used to determine whether or not there is functional signal loss when mapping functional data to a reference coordinate system, develop algorithmic solutions to reduce shape collapse problems and to determine the validity of population shape measurements when using nonrigid image registration methods. We showed that changing the smoothing kernel using SyN reduced the shape collapse in our example, but it still gave poor correspondence. This study suggests that we still have more to do to reduce shape collapse and improve registration.

One of the future things to do is to do a power analysis. For example, suppose

10 out 30 subjects have shape collapse problem at a point, we need to evaluate the loss of statistical power of statistical inferences at that point caused by shape collapse. One simple way to reduce the effect of shape collapse on statistical power is to throw away subjects with collapse at a that point. We also need to come up with efficient ways to reduce shape collapse and perverse the correspondence accuracy. One way to fix the collapse problem is to have multiple atlases (targets images). For example, in our region of interest, some atlases have a single sulcus, some atlases may have parallel sulcus, some atlases may have a "fork-shape" sulcus; some atlases may have one interrupted sulcus and other atlases may not have a sulcus.

REFERENCES

[1] B. B. Avants, C. L. Epstein, M. Grossman, and J. C. Gee. Symmetric diffeomorphic image registration with cross-correlation: evaluating automated labeling of elderly and neurodegenerative brain. *Med Image Anal*, 12(1):26–41, Feb 2008.

[2] Brian B Avants, Nicholas J Tustison, Gang Song, Philip A Cook, Arno Klein, and James C Gee. A reproducible evaluation of ants similarity metric performance in brain image registration. *Neuroimage*, 54(3):2033–2044, 2011.

[3] M.Faisal Beg, MichaelI. Miller, Alain Trouvé, and Laurent Younes. Computing large deformation metric mappings via geodesic flows of diffeomorphisms. *International Journal of Computer Vision*, 61(2):139–157, 2005.

[4] George TY Chen, Marc Kessler, and Samuel Pitluck. Structure transfer between sets of three dimensional medical imaging data. *Computer graphics*, 24:172–175, 1985.

[5] Benoit M Dawant, Steven L Hartmann, J-P Thirion, Frederik Maes, Dirk Vandermeulen, and Philippe Demaerel. Automatic 3-d segmentation of internal structures of the head in mr images using a combination of similarity and free-form transformations. i. methodology and validation on normal subjects. *IEEE transactions on medical imaging*, 18(10):909–916, 1999.

[6] Oguz C Durumeric, Ipek Oguz, and Gary E Christensen. The shape collapse problem in image registration. In *Mathematical Foundations of Computational Anatomy*, pages 95–106, 2013.

[7] Jim C Gee, Martin Reivich, and Ruzena Bajcsy. Elastically deforming 3d atlas to match anatomical brain images. *Journal of computer assisted tomography*, 17(2):225–236, 1993.

[8] Ali Ghayoor, Jatin G Vaidya, and Hans J Johnson. Development of a novel constellation based landmark detection algorithm. In *SPIE Medical Imaging*, pages 86693F–86693F. International Society for Optics and Photonics, 2013.

[9] Michael Halle, Ion-FlorinF. Talos, Marianna Jakab, Nikos Makris, Dominik Meier, Laurence Wald, Bruce Fischl, and Ron Kikinis. Multi-modality mri-based atlas of the brain. In *SPL*, 11 2015.

[10] Monica Hernandez, Matias N Bossa, and Salvador Olmos. Registration of anatomical images using geodesic paths of diffeomorphisms parameterized with stationary vector fields. In *2007 IEEE 11th International Conference on Computer Vision*, pages 1–8. IEEE, 2007.

[11] Derek LG Hill, David J Hawkes, JE Crossman, MJ Gleeson, TCS Cox, EECML Bracey, AJ Strong, and P Graves. Registration of mr and ct images for skull base surgery using point-like anatomical features. *The British journal of radiology*, 64(767):1030–1035, 1991.

[12] Marc L Kessler. Image registration and data fusion in radiation therapy. *The British journal of radiology*, 2014.

[13] Eun Young Kim and Hans J Johnson. Robust multi-site mr data processing: iterative optimization of bias correction, tissue classification, and registration. *Frontiers in neuroinformatics*, 7(29), 2013.

[14] Gerald Q Maguire Jr, Marilyn E Noz, Evan M Lee, and James H Schimpf. Correlation methods for tomographic images using two and three dimensional techniques. In *Information Processing in Medical Imaging*, pages 266–279. Springer, 1986.

[15] Calvin R Maurer and J Michael Fitzpatrick. A review of medical image registration. *Interactive image-guided neurosurgery*, 17, 1993.

[16] Michael I Miller, Gary E Christensen, Yali Amit, and Ulf Grenander. Mathematical textbook of deformable neuroanatomies. *Proceedings of the National Academy of Sciences*, 90(24):11944–11948, 1993.

[17] Julian G Rosenman, Elizabeth P Miller, Gregg Tracton, and Tim J Cullip. Image registration: an essential part of radiation therapy treatment planning. *International Journal of Radiation Oncology* Biology* Physics*, 40(1):197–205, 1998.

[18] Murray R Spiegel. Mathematical handbook of formulas and tables. 1968.

[19] Nathalie Strehl, Sandrine Tomei, Julian Rosenman, and Sarang Joshi. Large deformation 3d image registration in image-guided radiation therapy.

[20] J-P Thirion. Image matching as a diffusion process: an analogy with maxwell's demons. *Medical image analysis*, 2(3):243–260, 1998.

[21] Tom Vercauteren, Xavier Pennec, Aymeric Perchant, and Nicholas Ayache. Diffeomorphic demons: Efficient non-parametric image registration. *NeuroImage*, 45(1):S61–S72, 2009.